

ity) is again possible, with jumps between the different steady states accompanied by a critical slowing down, provided that the thermodynamic limit of an infinitely large lattice is taken *first* with respect to the long time limit. We argue that this order of limits is physically plausible, and we link the bistability to the fact that for finite size and time the probability distribution of relevant observables develops a strong bimodal structure. Depending on the order of limits, bimodality leads either to a first-order dissipative phase transition (as usually discussed when the long time limit is taken first), or to a bistable regime. We thus provide a theoretical scenario reconciling our results with the literature cited above, and finding similar dynamics in a model with Ising interactions (see below and App. B) indicates the generality of our results. We suggest that in an experimental platform based on trapped-ion quantum simulators, such a question can be addressed.

Model. We consider a quantum system with N sites $R \in \mathbb{Z}^D$ on a hypercubic lattice in D spatial dimensions, for which the connectivity is $\mathcal{Z} = 2D$. The master equation for ρ is defined using the Liouvillian $\hat{\mathcal{L}}$,

$$\partial_t \rho = \hat{\mathcal{L}}[\rho] \equiv -i[H, \rho] + \mathcal{D}[\rho], \quad \hbar = 1. \quad (1)$$

The Hamiltonian describing Rabi oscillations of two-level systems with a drive detuned by Δ from the resonant transition frequency and a Rabi frequency Ω , is given in a frame rotating with the drive by

$$H = \sum_R \left[\frac{\Delta}{2} \sigma_R^z + \Omega \sigma_R^x \right] - \sum_{\langle R, R' \rangle} J (\sigma_R^+ \sigma_{R'}^- + \text{h.c.}), \quad (2)$$

where the second sum extends over all pairs of NN sites, describing hopping with amplitude J , with spin- $\frac{1}{2}$ operators (Pauli matrices) σ_R^a , $a = \{x, y, z\}$, and $\sigma_R^\pm = (\sigma_R^x \pm i\sigma_R^y)/2$. For spin losses occurring independently at each site with rate $\Gamma = 1$ (which fixes the frequency and time units),

$$\mathcal{D}[\rho] = \sum_R \left[\sigma_R^- \rho \sigma_R^+ - \frac{1}{2} (\sigma_R^+ \sigma_R^- \rho + \rho \sigma_R^+ \sigma_R^-) \right]. \quad (3)$$

Aside from translation invariance, this model has no manifest microscopic symmetries. Its MF phase diagram displays bistability [46, 54] in a region of parameters that terminates at a second order point where an emerging Z_2 symmetry spontaneously breaks [37]. In 1D the steady state is unique as obtained by MPO simulations [54]. Here we focus on higher dimensions, which we find to manifest bistability in the thermodynamic limit.

Dynamics of Observables. From the master equation one can derive a hierarchy of equations of motion for n -points expectation values of the form $\langle \sigma_{R_1}^a \sigma_{R_2}^b \cdots \sigma_{R_n}^c \rangle \equiv \text{tr}\{\rho \sigma_{R_1}^a \sigma_{R_2}^b \cdots \sigma_{R_n}^c\}$, which depend on the value of correlators at the next order, $n + 1$. Assuming a translationally-invariant density matrix, we define the uniform vector mean magnetization, $\mu_a(t) =$

$\langle \frac{1}{N} \sum_R \sigma_R^a \rangle = \langle \sigma_R^a \rangle$, and its equations of motion

$$\partial_t \mu_x = -J\mathcal{Z}[\mu_y \mu_z + \eta_{yz}(1)] - \Delta \mu_y - \mu_x/2, \quad (4)$$

$$\partial_t \mu_y = J\mathcal{Z}[\mu_x \mu_z + \eta_{xz}(1)] - 2\Omega \mu_z + \Delta \mu_x - \mu_y/2, \quad (5)$$

$$\partial_t \mu_z = 2\Omega \mu_y - (1 + \mu_z). \quad (6)$$

with the connected two-point correlation functions,

$$\begin{aligned} \eta_{ab}(R, R', t) &\equiv \langle (\sigma_R^a - \mu_a) (\sigma_{R'}^b - \mu_b) \rangle \\ &= \langle \sigma_R^a \sigma_{R'}^b \rangle - \mu_a \mu_b, \quad R \neq R', \end{aligned} \quad (7)$$

and setting $R' = 0$ using the translation invariance, $\eta_{ab}(1)$ is the correlator at a NN of the origin.

Equations (4)-(6) are exact. The limit $\eta \rightarrow 0$ reduces ρ to a product of identical on-site states, leading to the MF equations, whose steady state and dynamics are studied in detail in [61]. We present an approximate scheme going beyond MF, formally based on an expansion in $1/\mathcal{Z}$ (with a related approach in [50]). Neglecting the connected three-point correlators $\langle (\sigma_R^a - \mu_a) (\sigma_{R'}^b - \mu_b) (\sigma_{R''}^c - \mu_c) \rangle \approx 0$, allows us to derive (see App. E) coupled equations for $\eta_{ab}(R, t)$, which we solve numerically together with their feedback into Eqs. (4)-(6). Since the short-range correlators $\eta_{ab}(1)$ appearing in Eqs. (4)-(6) are dynamically coupled to all distances in the lattice, the MFQF method accounts for the spatial structure of correlation functions. The simulations have been verified to converge as a function of N , and hence we can approximate the system dynamics as a function of time with the limit $N \rightarrow \infty$ taken first.

Correlations wash away Bistability in 1D. We start our analysis with numerically exact MPO calculations of large lattices in 1D. The density matrix ρ can be considered as a pure state in an enlarged Hilbert space with four states per site [62], allowing us to solve the Lindblad evolution using a method formally similar to pure state unitary evolution encoded using well-established matrix product states (see [63, 64] and references therein). We evolve $\rho(t)$ in a 1D chain with open BC (translation invariance is not enforced), using an MPO algorithm [53, 62, 65], with an implementation based on the iTensor library [66], a Trotter decomposition of order four [64, 67], and bond dimension $\chi = 300$. With up to 200 spins we checked that observables measured in the central region of the chain had negligible finite-size effects and truncation errors at the scale of the plots, allowing us to obtain their steady-state bulk values corresponding to the thermodynamic limit.

Figure 1(a) shows the x component of the steady-state magnetization, $\bar{\mu}^S \equiv \lim_{t \rightarrow \infty} \bar{\mu}(t)$, in 1D, for $J\mathcal{Z} = 4$ as a function of Δ . In MF, $\bar{\mu}^S$ is unique except for $1.3 \lesssim \Delta \lesssim 1.9$, where there are two co-existing stable solutions in addition to an unstable solution. At the presence of quantum correlations (in MPO and MFQF), the magnetization departs significantly from the MF prediction, with a crossover between the two limiting regimes, in the range $1.5 \lesssim \Delta \lesssim 5$. We define the inverse correlation lengths λ_{ab} by fitting the six correlation functions

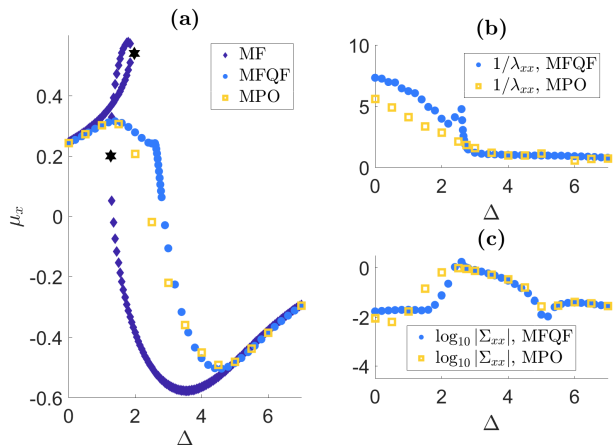


FIG. 1. (a) Mean steady-state x magnetization μ_x^S as a function of Δ for $\Omega = 0.5$ and $JZ = 4$, on a 1D lattice. The mean-field (MF) limit manifests bistability, with three co-existing solutions, two of which – those on the branches coming from the limits of $\Delta \rightarrow \{0, \infty\}$, are stable. Two black hexagrams mark the points where the unstable branch meets each of the two stable ones. An exact numerical treatment using Matrix Product Operators (MPO) shows a crossover within a range of Δ shifted from the MF bistability region. An approximation incorporating quantum fluctuations at leading order (MFQF) follows approximately the MPO result in a large range of parameters. (b) The correlation length λ_{xx} defined by fitting $\eta_{xx} \sim \exp\{-\lambda_{xx}R\}$, and (c) the total correlation $\Sigma_{xx} = \sum_R \eta_{xx}(R)$, calculated in MPO and MFQF, showing that the latter approximation is capable of capturing the spatial structure and relative magnitudes of two-point correlations in the lattice.

to $\eta_{ab}(R) \sim \exp\{-\lambda_{ab}R\}$. For simplicity, we present in Fig. 1(b) only one correlation length, and Fig. 1(c) shows the corresponding total correlation measured by $\Sigma_{ab} = \sum_R \eta_{ab}(R)$. The spatial structure of the two-point correlation undergoes a sharp change within the crossover region, from relatively small but widely extended correlations for low Δ , to much larger but very short-ranged correlations, for high Δ . A separate analysis of the correlations shows that at the same time, the correlations change nature from periodic modulations (spin density-wave character), to being overdamped in space.

As Fig. 1 shows, the MFQF approximation correctly captures the uniqueness of the steady state and the disappearance of bistability in 1D. On both sides of the crossover region, the results are quantitatively accurate. In its center, the approximation reaches too large values for $\eta_{ab}(R)$ and the correlation length. More generally, we find that as J is increased in 1D, the MFQF approach loses its accuracy (for parameters of strong correlations), plausibly because of the role of higher-order correlation functions that are neglected, which can lead at much larger J to the breakdown of the approximation. However, the MFQF approach is easy to generalize to higher dimensions, and quantitatively accurate in regions with moderate correlations.

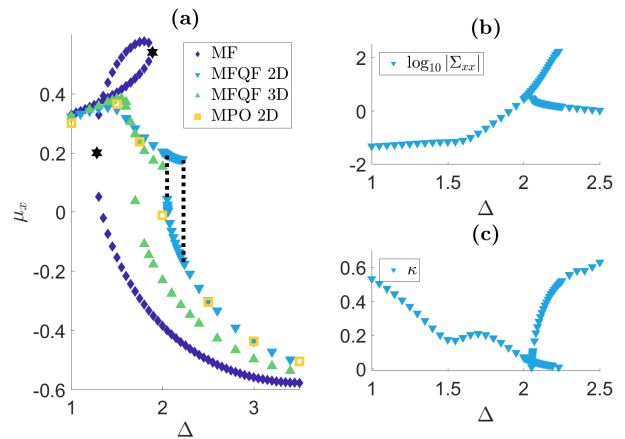


FIG. 2. (a) Mean steady-state x magnetization μ_x^S in the MFQF $N \rightarrow \infty$ approximation in 2D-3D, together with the MF limit and 2D-MPO results (for a 12×4 cylinder). The parameters are as in Fig. 1, with JZ kept fixed by varying J with the dimension. For $D \geq 2$ MFQF predicts multistability, with two stable branches approaching the MF branches in an increasingly larger parameter region as D is increased. The dotted black lines indicate the edges of the 2D bistable region. The simulations were run with lattices of up to 200^2 and 40^3 sites and periodic BC. (b) The total correlation in 2D, showing a difference of up to two orders of magnitude in the bistable phases. (c) The rate of convergence to the 2D steady states, fitted to an exponential form $\sim e^{-\kappa t}$, showing a critical slowing down of the dynamics as $\kappa \rightarrow 0$ at the two bistability edges.

Bistability in Higher dimensions. Figure 2(a) shows the results of simulations with large 2D and 3D lattices, for $JZ = 4$. The MFQF theory, that allows simulating large lattices (with $N \rightarrow \infty$), is compared with 2D-MPO calculations, limited to a finite-size system, for which, as in 1D, ρ is encoded as a product of matrices. The matrix product runs over a snake-like path visiting all the sites of a cylinder of length $L_x = 12$ and perimeter $L_y = 4$ (see App. C). Such an approach has been applied in ground-state calculations of 2D models [68], but we are not aware of previous 2D-MPO Lindblad calculations. For $\Delta \lesssim 1.5$ and $\Delta \gtrsim 2.5$ the agreement between MPO and MFQF is almost perfect, giving a nontrivial check of the ability of MFQF to capture significant correlation effects (that result in $\bar{\mu}$ strongly departing from MF). The computational cost of guaranteeing a high accuracy in 2D-MPO calculation is exponential in L_y (see App. C), limiting the present MPO calculations to relatively small systems, which cannot show bistability (and a possible discontinuity would also be smeared out).

As our main result, using MFQF we find in 2D two stable $\bar{\mu}^S$ branches, that in 3D extend over larger ranges of Δ , converging towards the MF bistability region and magnetization values. Figure 2(b) shows that Σ_{xx} increases by two orders of magnitude for one of the bistable states, and Fig. 2(c) shows the asymptotic relaxation rate associated to the convergence to $\bar{\mu}^S$. It is obtained by fit-

ting $\partial_t \bar{\mu}^2 \sim e^{-\kappa t}$ at large times ($t \sim 100$). The fact that $\kappa \rightarrow 0$ at the branch edges in 2D indicates a critical slowing down when approaching the end of the bistability region in the phase that is about to disappear, leading to a discontinuous jump. The MFQF approach does however not *always* predict bistability in 2D. Replacing each hopping term in Eq. (2) by the Ising coupling $J_z \sigma_R^z \sigma_{R'}^z$, we find a smooth crossover for moderate J_z (as obtained using cluster meanfield [56]), and a small bistability region for stronger couplings (again as in [56]); See App. B.

Bistability, Liouvillian spectrum and bimodality. We henceforth return to the question raised in the introduction: how to reconcile the uniqueness of the steady state in finite systems, with bistability seen when taking first the thermodynamic limit of infinite size, and then the long-time limit?

Considering the Liouvillian $\hat{\mathcal{L}}$ of Eq. (1), the unique thermodynamic steady state corresponds to $\rho_{ss} = \lim_{N \rightarrow \infty} \lim_{t \rightarrow \infty} \rho(t)$, which is independent of the initial conditions, and is an eigenstate of $\hat{\mathcal{L}}$ at any N , $\hat{\mathcal{L}}\rho_{ss} = 0$. Assuming bistability, we define ρ_1 and ρ_2 as the two distinct density matrices obtained from $\lim_{t \rightarrow \infty} \lim_{N \rightarrow \infty} \rho(t)$, which depend on the initial conditions. For N large but finite the bistability should be replaced by long-lived metastable states, in which case ρ_1 and ρ_2 are defined at times $t \gg 1/\Gamma$, but small compared to the lifetime of these metastable states. As in the model studied here, these two states have different local properties: a local observable (*i.e.* sum of local terms, e.g. $M_x = \frac{1}{N} \sum_R \sigma_R^x$) has a probability distribution $P_1(m)$ with a single peak centred around m_1 in ρ_1 , and a distribution $P_2(m)$ peaked around $m_2 (\neq m_1)$ in ρ_2 . At the same time, metastability implies some relaxation time diverging with N , and the spectrum of $\hat{\mathcal{L}}$ must have at least one nonzero eigenvalue λ_E with a vanishingly small real part, $\lim_{N \rightarrow \infty} \text{Re}(\lambda_E) = 0$, other eigenvalues being separated by a gap $\mathcal{O}(\Gamma)$ [59, 69]. We assume for simplicity that $\hat{\mathcal{L}}$ has a unique such small eigenvalue (therefore real), and denote by ρ_E the associated eigenstate (or eigenmatrix). ρ_{ss} and ρ_E are the eigenstates from which all long-lived states can be constructed, since for t much larger than $1/\Gamma$ we can ignore higher “excited” eigenstates. So, for ρ_1 and ρ_2 to be long-lived, they must be linear combinations of ρ_{ss} and ρ_E . As physical states have a trace equal to 1, and since $\text{Tr}\rho_{ss} = 1$ and $\text{Tr}\rho_E = 0$, there must exist two distinct scalars a_1 and a_2 such that $\rho_i = \rho_{ss} + a_i \rho_E$ with $i = 1, 2$ [39, 48, 59, 69]. Inverting these relations we get $\rho_{ss} = (a_2 \rho_1 - a_1 \rho_2)/(a_2 - a_1)$. So, if a_1 and a_2 are both nonzero (which may not be always the case) ρ_{ss} is a “cat state” (with correlation functions extending over the system size), being a linear combination of two uniform physical states with different local properties. In ρ_{ss} , the probability distribution $P_{ss} = (a_2 P_1 - a_1 P_2)/(a_2 - a_1)$ of a local observable is *bimodal*, peaked around the two mean values $m_{1,2}$ realized in the states $\rho_{i=1,2}$.

Using exact diagonalization on small systems we have computed such distributions for the fully-connected (FC)

version of the present XY model, which is bistable in the thermodynamic limit (where MF becomes exact), and for the 1D and 2D cases. We find (App. A), that the magnetization becomes bimodal in parts of the MF bistability region for the FC and 2D cases, whereas it stays monomodal in 1D. The scaling with N of the bimodal peaks is beyond the scope of the current work, however, the mean value of an observable computed with ρ_{ss} may become *discontinuous* as $N \rightarrow \infty$ at some value of the parameter [43, 48, 55, 70]. This could correspond, in the discussion above, to smoothly varying $\rho_{i=1,2}$ but discontinuous jumps of a_1 and a_2 . Hence, a unique steady state with a discontinuous jump is a-priori compatible with bistability and hysteresis and, in the present scenario, finding one or the other in a theory calculation is a matter of order of limits.

Moreover, since the support of P_1 has essentially no overlap with that of P_2 (for a large enough system), any density matrix which is not a convex combination of ρ_1 and ρ_2 would give some (unphysical) negative probability density. This means that all physical long-lived states are convex combinations of the mono-modal states ρ_i , and the latter thus coincide with the extreme states of [59]. The above discussion therefore connects our results both with the theories of first-order phase transitions, and the theory based on the extreme metastable states. The lifetimes of the many-body metastable states would diverge with N , plausibly $\propto e^N$, and for large enough N , exceed the time accessible in numerical or experimental realizations. We conjecture that an initial state with a finite correlation length will lead, in the time window $1/\Gamma \ll t \ll 1/|\lambda_E|$, to one of the two mono-modal states ρ_i , and *not* to an arbitrary combination of the two. A heuristic argument is given in App. D. A product state is a natural reproducible initial state in an experiment, allowing to explore the metastability. As a parameter is swept back and forth across the bistability region in an experimental setup, observables will show hysteresis loops – unless the sweep is unrealistically slow ($\propto e^{-N}$).

Experimental feasibility. In addition to possible realizations with circuit-QED arrays [54], driven-dissipative spin models can be realized in current experiments with a few tens to a few hundreds of trapped ions. Ising and XY interactions can be implemented by laser beams inducing spin-motion coupling along one or two orthogonal directions [71–73], with an additional laser for the on-site Hamiltonian. As recently demonstrated experimentally, the interaction can be varied from being almost independent of distance to a dipolar power-law, and therefore short-range in 1D [74, 75] and 2D lattices [26]. The interaction strength in these works is of order $J/\hbar \sim 10^4 s^{-1}$, one to two orders of magnitude larger than the qubit dephasing rates, and the rate of spin-flip processes in Eq. (3) can be potentially controlled as well.

To conclude, studying lattices of driven-dissipative interacting spins using state-of-the-art 1D MPO simulations, for the parameters presented here and in further parameter regimes [61], we have found no phase transi-

tion but a crossover between two regimes with different characteristics. On the other hand, using a new approach that accounts for the leading-order lattice correlations and their feedback onto the mean magnetization, bistability appears to be possible in driven-dissipative quantum systems already in 2D. Thus, the present exact and approximate calculations suggest that $D = 2$ is a lower critical dimension for bistability in this problem. This conclusion is consistent with works done in the context of Rydberg atoms on related models [37], pointing toward a model-A dynamic universality class (whose lower critical dimension is known to be two) for the second order phase transition at the ending point of the bistability regime. This implies that in one dimension fluctuations destroy the critical point and with it the entire bistability region, in line with our results.

The question of the existence of a lower critical dimension for bistability, bimodality and hysteresis and the accompanied dissipative phase transitions in this model can be directly addressed experimentally. If a definite answer is found, it would constitute the first demonstration of deciding a question currently intractable classically, by a controlled quantum simulation. It could ascertain the status of the meanfield approximation in these systems, and shed light on the differences between equilibrium and nonequilibrium phase transitions.

ACKNOWLEDGMENTS

We acknowledge the DRF of CEA for providing us with CPU time on the supercomputer COBALT of the CCRT. H.L. thanks Roni Geffen for fruitful discussions, and acknowledges support by IRS-IQUPS of Université Paris-Saclay and by LabEx PALM under grant number ANR-10-LABX-0039-PALM.

Appendix A: Bimodality

We start studying the model of Eqs.(1)-(3) of the main text on a finite FC lattice with N sites, i.e. a graph where all sites are linked (with connectivity $\mathcal{Z} = N - 1$). The FC version of the model is interesting because: (i) it has a unique steady state for any finite N , (ii) its mean-field (MF) solution gives a set of non-linear differential equations which can support bistability, and (iii) the MF approximation becomes asymptotically exact in the limit $N \rightarrow \infty$. This is due to the fact that each site is coupled to the x and y components of the total magnetization of the $N - 1$ other sites, and the fluctuations of this magnetization generically become small compared to its mean when $N \rightarrow \infty$. As the thermodynamic limit $N \rightarrow \infty$ is approached, the bistability is thus expected to appear in some way and the FC model can be viewed as a playground to investigate how a unique steady state at finite N can be reconciled with bistability in the thermodynamic limit.

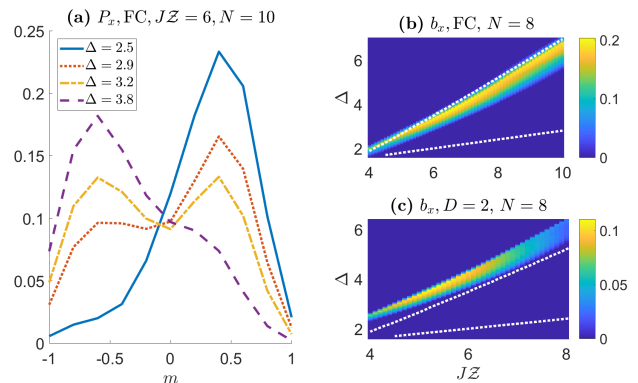


FIG. 3. (a) Probability distribution $P_x = P(M_x = m)$ of the x magnetization per-site ($M_x = \frac{1}{N} \sum_R \sigma_R^x$), for a few values of the detuning Δ , at fixed $J\mathcal{Z}$ and $\Omega = 0.5$, in the steady state of the XY model with $N = 10$ spins on a fully connected (FC) lattice. The transition from a single peak centered at $m > 0$ to a single peak at $m < 0$ as Δ is increased, is accompanied by an intermediate region of a bimodal distribution. (b) The bimodality index b_x (see text) given by the color code, with $\Omega = 0.5$ and $N = 8$ for the FC lattice. Within the region bounded by the two white dotted lines, the mean-field limit manifests bistability of two different steady-state magnetizations. (c) b_x for a two-dimensional (2D) parallelogram of $N = 8$ sites and periodic boundary conditions (note the smaller $J\mathcal{Z}$ range). We find bimodality, although weaker than in the FC model, and with stronger finite-size effects.

We thus compute exactly the unique stationary state density matrix $\rho_{ss} = \lim_{t \rightarrow \infty} \rho(t)$ on small systems. We focus on the probability distribution of the x magnetization per site, i.e. $P_x = P(M_x = m)$, where $M_x = \frac{1}{N} \sum_R \sigma_R^x$, that we plot in Fig. 3(a) at fixed Ω and $J\mathcal{Z}$ (the rescaling by \mathcal{Z} allows to compare lattices of a different connectivity), and for different values of Δ . Quite interestingly, such probability distribution evolves from a single peak centered around $m > 0$ to a single peak centered around $m < 0$, with an intermediate Δ range where P_x has two separated peaks. To quantify the bimodality of the distribution we define an index $b_x = 2(P_{\max,2} - P_{\min}) / (P_{\max,1} + P_{\max,2})$, where $P_{\max,2} \leq P_{\max,1}$ are the two maxima of the distribution, and P_{\min} is the minimum between the two. As can be seen in Fig. 3(b), the extent of the bimodality region in Δ and the maximum of b_x increase with $J\mathcal{Z}$ at a fixed Ω , following the MF bistability region.

While in the finite size limit we consider here the stationary state is still unique and the average value of the observable will either evolve smoothly with Δ or give rise to a step, depending on the scaling with N of the peaks, the emergence of a bimodal probability distribution suggests a possible scenario for bistability to survive. Indeed for a FC lattice taking the thermodynamic limit first leads to a set of non-linear differential equations which can support multiple stable solutions. This should translate, in the probability distribution of the magnetization at finite size and finite time, and depend-

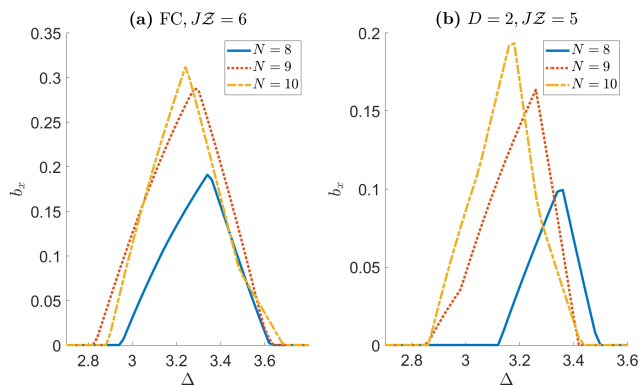


FIG. 4. The bimodality index b_x (see text) as a function of Δ for (a) $J\mathcal{Z} = 6$ in a fully-connected (FC) lattice, and (b) $J\mathcal{Z} = 5$ in a 2D lattice, from exact numerical solutions of the master equation of the driven-dissipative XY model, for small lattices, with three values of $N = 8, 9, 10$.

ing on the initial condition, in the emergence of a second peak on time scales exponentially in the system size such that, in the thermodynamic limit the switching from one solution to the other becomes exponentially suppressed.

Repeating this analysis for a 2D square lattice with periodic boundary conditions (BC) we find again a bimodal parameter region, shifted towards higher Δ , with and the maximum b_x smaller than in the FC model [Fig. 3(c)]. With an increasing interaction strength J , the magnitude and extent of correlated fluctuations in the lattice grow, explaining the gradual decrease of the bimodal parameter region for a small lattice. As further consistency checks, we verified that when increasing N (up to 10) at specific parameter values, the bimodality range and maximum increase, and for a 1D chain we find (not shown) that b_x remains strictly zero.

Figure 4 shows the bimodality index b_x calculated exactly for three increasing lattice sizes (in the 2D case shown in panel (b), different parallelograms are constructed with periodic boundary conditions to incorporate N sites), for the driven-dissipative XY model discussed in the main text. Although sensitive to the finite system size, the width of the Δ ranges of bimodality increase with N and the maximal b_x value increases accordingly, which is consistent with bistability in the $N \rightarrow \infty$ limit.

Appendix B: Bistability in a driven-dissipative Ising model in 2D

We have employed the MFQF method to the study of the driven dissipative Ising model, obtained after replacing the XY (flip-flop) interaction term in the Hamiltonian,

$$H = \sum_R \left[\frac{\Delta}{2} \sigma_R^z + \Omega \sigma_R^x \right] - \sum_{\langle R, R' \rangle} \frac{J_z}{2} \sigma_R^z \sigma_{R'}^z, \quad (\text{B1})$$

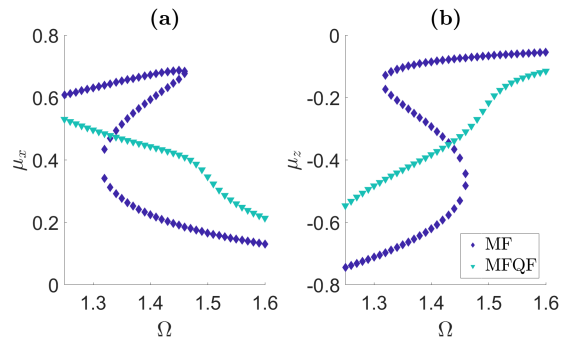


FIG. 5. (a) Mean steady-state x magnetization μ_x^S as a function of Ω for $\Delta = 0$ and $J_z\mathcal{Z} = -4$, on a 2D lattice for the Ising model. (b) The mean steady-state z magnetization for the same parameters. The MF manifests bistability in the Ω range shown, while MFQF predicts a smooth crossover. We note that in the notation of Ref. [56], $\Omega = (h_x/\gamma)/2$, and $J_z\mathcal{Z} = -V/\gamma$ and the current figure corresponds to Fig. 1(a) of Ref. [56], in a somewhat larger Ω range, showing a rather sharp change around $\Omega \approx 1.5$. The simulation accounts for a lattice of 100^2 sites, and the results have been verified to converge in N and t .

while keeping the dissipator identical. The equations of motion for $\vec{\mu}$ that are obtained from this model are identical to those in Eqs. (4)-(6) of the main text with just the replacement $J \rightarrow -J_z$. The correlator equations (given in the following), are different.

Setting $\Delta = 0$ we have studied the resulting MFQF steady state on a 2D lattice. A necessary condition for bistability in the meanfield limit [61], is $|J_z\mathcal{Z}| > 2$. For $J_z\mathcal{Z} = -4$, Fig. 5 shows a smooth crossover of the steady-state magnetization $\vec{\mu}^S$ as a function of Ω across the parameter region of meanfield bistability. The z magnetization curve of Fig. 5(b) can be compared with the results plotted in Fig. 1(a) of [56], which were obtained using a cluster MF approach for different cluster sizes. In the notation of Ref. [56], $J_z\mathcal{Z} = -V/\gamma$ and $\Omega = (h_x/\gamma)/2$, making the parameters in the plots identical (with only a somewhat larger range taken here for the abscissa). The MFQF curve that we obtain contains a further noticeable feature around $\Omega \approx 1.5$, with a relatively sharper change in magnetization.

In Fig. 6, μ_x^S and μ_z^S are shown for $J_z\mathcal{Z} = -6$, in a larger region of Ω across the parameter region of meanfield bistability. The z magnetization curve of Fig. 6(b) can be compared with the curves plotted in Fig. 1(b) of [56]. In the region where the cluster MF of Ref. [56] predicts a shrinking of the bistability (but not its complete disappearance up to the largest available cluster size), MFQF predicts a rather sharp but smooth crossover. However in MFQF approach bistability remains in a small region ($2.06 \lesssim \Omega \lesssim 2.13$), at the right edge of MF bistability region. The structure of these the two co-existing stable phases is distinctly different in terms of the correlation functions $\eta_{ab}(R)$ defined in Eq. (7) of the main text. Figure 7 presents the characteristics of $\eta_{zz}(R)$

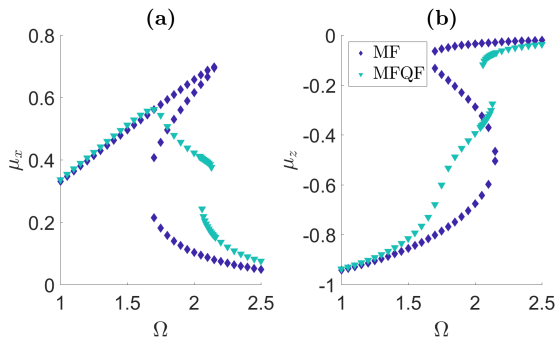


FIG. 6. (a) Mean steady-state x magnetization μ_x^S as a function of Ω for $\Delta = 0$ and $J_z \mathcal{Z} = -6$, on a 2D lattice for the Ising model. (b) The mean steady-state z magnetization for the same parameters. The MF manifests bistability in the large Ω range shown, while MFQF predicts a shrinking of the bistability region and its occurrence at the edge of the Ω range. We note that in the notation of Ref. [56], $\Omega = (h_x/\gamma)/2$, and $J_z \mathcal{Z} = -V/\gamma$ and the current figure corresponds to Fig. 1(b) of Ref. [56]. The simulation accounts for a lattice of 100^2 sites, and the results have been verified to converge in N and t . See Fig. 7 for the characteristics of correlation functions around the bistable region.

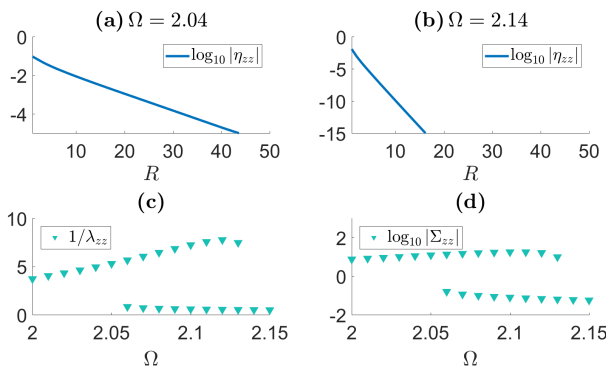


FIG. 7. Characteristics of the correlation functions around the bistable region of Fig. 6. (a)-(b) The correlation function $\eta_{zz}(R)$ as a function of the distance for two different Ω values (outside the bistability region). Note the different scales of the two plots. (c) The correlation length (along one spatial direction) as a function of Ω , showing a difference of up to an order of magnitude in the bistable phases. (d) The total correlation $\Sigma_{zz} = \sum_R \eta_{zz}$, showing a difference of up to two orders of magnitude in the bistable phases.

as an example, showing the large differences in the correlation length, and – as a result – the total correlation, between the two bistable states.

Appendix C: 2D-MPO

The 2D MPO calculations presented in Fig. 3 of the main text and in Fig. 8, have been carried out on cylinders of length L_x from 8 to 16, and fixed $L_y = 4$. At fixed precision the required bond dimension χ is expected to

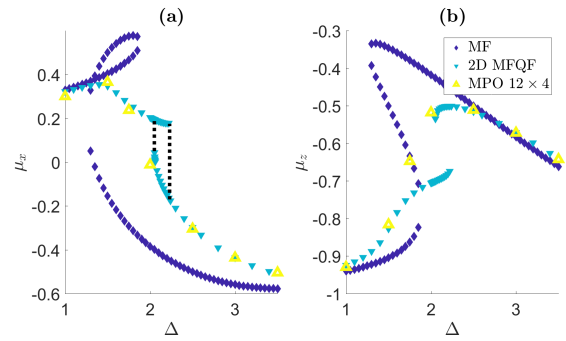


FIG. 8. (a) Mean steady-state x magnetization μ_x^S and (b) z magnetization μ_z^S , in the MFQF approximation in 2D, together with the MF limit and 2D-MPO results (for a finite-size, 12×4 cylinder). The parameters are as in Fig. 3 of the main text.

be constant with L_x , but exponentially large in L_y . The data is obtained with a bond dimension $\chi = 400$ (pushed to $\chi = 600$ at $\Delta = 1.75$). As in the 1D-MPO result, the steady state is obtained by evolving ρ in time from an initial state where all the spins are pointing down. In practice a total time between 15 and 25 was used. Since the path of interacting spins associated to the MPO artificially breaks the translation invariance of the lattice in the y direction, it is important to check that the bond dimension is large enough to restore the translation symmetry in the observables. In our case the magnetization was found to be translation invariant up to relative errors of the order of $\mathcal{O}(10^{-4})$.

Appendix D: Finite correlation length and mono-modal states

Consider a system where the Liouvillian spectrum has a steady state ρ_{ss} , associated to the eigenvalue 0, and an eigenstate ρ_E associated to an eigenvalue λ_E which goes to zero when increasing the system size. We assume that all the other eigenstates are gapped and can be ignored for times $t \gg 1/\Gamma$. As discussed in the main text, there exists two special linear combinations $\rho_{i=1,2}$ of ρ_{ss} and ρ_E , which are the extreme states [56], and in which local observables have probability distributions with a single peak. On the other hand, nontrivial linear combinations of ρ_1 and ρ_2 host bimodal distributions. A natural question is then: what initial conditions lead to ρ_1 and ρ_2 , and what initial conditions instead lead to some convex combination of the two? We give below a simple heuristic argument suggesting that initial conditions where connected correlation functions have a finite correlation length, should, for a large enough system, lead to one of the two extreme states and *not* to arbitrary convex combinations of the two. Take an initial state $\rho(t=0)$ where all connected correlation functions are short-ranged. Thanks to the assumption of a gap in the Liouvillian spectrum (above $|\lambda_E|$), the state

$\rho(t)$ will reach the metastable manifold (spanned by ρ_{ss} and ρ_E) rather quickly, after a time scale of order $\mathcal{O}(N^0)$, *i.e.* a time that is not growing with the system size. Because lattice models with short-range interactions typically have a maximum (Lieb-Robinson) velocity, beyond which the information cannot propagate, it should not be possible for the system to develop true long-range correlations (spanning the whole system) in a finite amount of time. And if correlations remain negligible at distances comparable with the system size, then this implies that the probability distributions of local observable cannot be bi-modal. So, the Lindblad dynamics of a large system initialized from a state with short-range correlations cannot lead to a bimodal state in the time range $1/\Gamma \ll t \ll N^{1/D}$ ($N^{1/D}$ is proportional to the linear size of the system). We thus conclude that in this time window the state that is reached is close to one of the two extreme states, since any other convex combination would be bimodal.

Appendix E: Meanfield with Quantum Fluctuations

To derive the equations of the MFQF approach, we define a two-point correlation function (correlator),

$$\vartheta_{ab}(R, R', t) \equiv \langle \sigma_R^a \sigma_{R'}^b \rangle, \quad R \neq R', \quad (\text{E1})$$

which is a function of the difference $R - R'$ alone, symmetric in a, b (because σ_R^a and $\sigma_{R'}^b$ commute). Using Eq. (E1), the connected two-point correlator is defined as in Eq. (7) of the main text, for $R \neq R'$, by

$$\eta_{ab}(R, R', t) = \vartheta_{ab}(R, R') - \mu_a \mu_b, \quad (\text{E2})$$

The connected three-point correlator is defined for $R \neq R' \neq R''$ by

$$\zeta_{abc}(R, R', R'', t) \equiv \langle (\sigma_R^a - \mu_a) (\sigma_{R'}^b - \mu_b) (\sigma_{R''}^c - \mu_c) \rangle, \quad (\text{E3})$$

which is again a function of the differences only.

The approximation of the following treatment is based on assuming that ζ (and higher order connected correlators) can be neglected in comparison to η . The e.o.m of ϑ_{ab} , setting $R' = 0$, is

$$\begin{aligned} \partial_t \vartheta_{ab}(R) = \\ \sum_d \Pi_{ad} \vartheta_{db}(R) + \sum_d \Pi_{bd} \vartheta_{ad}(R) + f_{ab}(\mu, \vartheta) + g_{ab}(\mu, \vartheta), \end{aligned} \quad (\text{E4})$$

where the local Hamiltonian terms are described using the matrix

$$\Pi = \begin{pmatrix} 0 & -\Delta & 0 \\ \Delta & 0 & -2\Omega \\ 0 & 2\Omega & 0 \end{pmatrix}, \quad (\text{E5})$$

while $f_{ab}(\mu, \vartheta) \propto J$ comes from the kinetic terms, and $g_{ab}(\mu, \vartheta) \propto \Gamma$ comes from the Lindbladian part, and both are given below. By using Eq. (E2) we get the e.o.m system for $\eta(R, t)$,

$$\partial_t \eta_{ab}(R, t) = \partial_t \vartheta_{ab}(R) - \partial_t [\mu_a \mu_b], \quad (\text{E6})$$

which we solve numerically together with the coupled system for $\vec{\mu}(t)$.

For the Hamiltonian in Eq. (2) of the main text where the kinetic term is

$$- \sum_{\langle R, R' \rangle} J (\sigma_R^+ \sigma_{R'}^- + \text{h.c.}) = - \sum_{\langle R, R' \rangle} \frac{J}{2} (\sigma_R^x \sigma_{R'}^x + \sigma_R^y \sigma_{R'}^y), \quad (\text{E7})$$

we find that $f_{ab}(\mu, \vartheta)$ of Eq. (E4) is given by,

$$f_{xx}(R) = 2J [2\mu_x \mu_y \mu_z - \mu_x \vartheta_{yz}(1) - \mu_y \vartheta_{xz}(R)] [\mathcal{Z} - \delta_{\|R\|,1}] - 2J \sum_{\substack{R' \neq 0 \\ \|R' - R\|=1}} \mu_z \vartheta_{xy}(R'), \quad (\text{E8})$$

$$f_{yy}(R) = -2J [2\mu_x \mu_y \mu_z - \mu_y \vartheta_{xz}(1) - \mu_x \vartheta_{yz}(R)] [\mathcal{Z} - \delta_{\|R\|,1}] + 2J \sum_{\substack{R' \neq 0 \\ \|R' - R\|=1}} \mu_z \vartheta_{xy}(R'), \quad (\text{E9})$$

$$f_{zz}(R) = -2J [\mu_x \vartheta_{yz}(R) - \mu_y \vartheta_{xz}(R)] [\mathcal{Z} - \delta_{\|R\|,1}] - 2J \sum_{\substack{R' \neq 0 \\ \|R' - R\|=1}} [\mu_y \vartheta_{xz}(R') - \mu_x \vartheta_{yz}(R')]. \quad (\text{E10})$$

$$\begin{aligned} f_{xy}(R) = J [2\mu_y^2 \mu_z - 2\mu_x^2 \mu_z - \mu_y \vartheta_{yz}(1) - \mu_y \vartheta_{yz}(R) + \mu_x \vartheta_{xz}(1) + \mu_x \vartheta_{xz}(R)] [\mathcal{Z} - \delta_{\|R\|,1}] \\ - J \sum_{\substack{R' \neq 0 \\ \|R' - R\|=1}} [\mu_z \vartheta_{yy}(R') - \mu_z \vartheta_{xx}(R')], \end{aligned} \quad (\text{E11})$$

$$f_{xz}(R) = -J\mu_y\delta_{\|R\|,1} + J [2\mu_z^2\mu_y - \mu_z\vartheta_{yz}(1) - \mu_y\vartheta_{zz}(R) - \mu_x\vartheta_{xy}(R) + \mu_y\vartheta_{xx}(R)] [\mathcal{Z} - \delta_{\|R\|,1}] - J \sum_{\substack{R' \neq 0 \\ \|R'-R\|=1}} [\mu_z\vartheta_{yz}(R') + \mu_y\vartheta_{xx}(R') - \mu_x\vartheta_{xy}(R')], \quad (\text{E12})$$

$$f_{yz}(R) = J\mu_x\delta_{\|R\|,1} + J [-2\mu_z^2\mu_x + \mu_z\vartheta_{xz}(1) + \mu_x\vartheta_{zz}(R) - \mu_x\vartheta_{yy}(R) + \mu_y\vartheta_{xy}(R)] [\mathcal{Z} - \delta_{\|R\|,1}] + J \sum_{\substack{R' \neq 0 \\ \|R'-R\|=1}} [\mu_z\vartheta_{xz}(R') - \mu_y\vartheta_{xy}(R') + \mu_x\vartheta_{yy}(R')]. \quad (\text{E13})$$

The components of $g(\mu, \vartheta)$ in Eq. (E4) are given by

$$g_{aa} = -\Gamma\vartheta_{aa}, \quad g_{xy} = -\Gamma\vartheta_{xy}, \quad g_{xz} = -\Gamma \left[2\vartheta_{xz} + \frac{3}{2}\mu_x \right], \quad g_{yz} = -\Gamma \left[2\vartheta_{yz} + \frac{3}{2}\mu_y \right]. \quad (\text{E14})$$

For the Ising model of Eq. (B1) where the kinetic term is

$$- \sum_{\langle R, R' \rangle} \frac{J_z}{2} \sigma_R^z \sigma_{R'}^z, \quad (\text{E15})$$

we get instead of the above $f_{ab}(\mu, \vartheta)$, the following expressions;

$$f_{xx}(R) = -2J_z [2\mu_x\mu_y\mu_z - \mu_x\vartheta_{yz}(1) - \mu_z\vartheta_{xy}(R)] [\mathcal{Z} - \delta_{\|R\|,1}] + 2J_z \sum_{\substack{R' \neq 0 \\ \|R'-R\|=1}} \mu_y\vartheta_{xz}(R'), \quad (\text{E16})$$

$$f_{yy}(R) = 2J_z [2\mu_x\mu_y\mu_z - \mu_y\vartheta_{xz}(1) - \mu_z\vartheta_{xy}(R)] [\mathcal{Z} - \delta_{\|R\|,1}] - 2J_z \sum_{\substack{R' \neq 0 \\ \|R'-R\|=1}} \mu_x\vartheta_{yz}(R'), \quad (\text{E17})$$

$$f_{zz}(R) = 0. \quad (\text{E18})$$

$$f_{xy}(R) = J_z [2\mu_x^2\mu_z - 2\mu_y^2\mu_z - \mu_x\vartheta_{xz}(1) - \mu_z\vartheta_{xx}(R) + \mu_y\vartheta_{yz}(1) + \mu_z\vartheta_{yy}(R)] [\mathcal{Z} - \delta_{\|R\|,1}] + J_z \sum_{\substack{R' \neq 0 \\ \|R'-R\|=1}} [\mu_y\vartheta_{yz}(R') - \mu_x\vartheta_{xz}(R')], \quad (\text{E19})$$

$$f_{xz}(R) = J_z\mu_y\delta_{\|R\|,1} - J_z [2\mu_z^2\mu_y - \mu_z\vartheta_{yz}(1) - \mu_z\vartheta_{yz}(R)] [\mathcal{Z} - \delta_{\|R\|,1}] + J_z \sum_{\substack{R' \neq 0 \\ \|R'-R\|=1}} \mu_y\vartheta_{zz}(R'), \quad (\text{E20})$$

$$f_{yz}(R) = -J_z\mu_x\delta_{\|R\|,1} + J_z [2\mu_z^2\mu_x - \mu_z\vartheta_{xz}(1) - \mu_z\vartheta_{xz}(R)] [\mathcal{Z} - \delta_{\|R\|,1}] - J_z \sum_{\substack{R' \neq 0 \\ \|R'-R\|=1}} \mu_x\vartheta_{zz}(R'). \quad (\text{E21})$$

-
- [1] S. Haroche and J. Raimond, *Exploring the Quantum: Atoms, Cavities, and Photons*, 1st ed. (Oxford University Press, USA, 2006).
- [2] Y. Yamamoto, F. Tassone, and H. Cao, *Semiconductor Cavity Quantum Electrodynamics*, 1st ed. (Springer, 2000).
- [3] R. J. Schoelkopf and S. M. Girvin, “Wiring up quantum systems,” *Nature* **451**, 664 (2008).
- [4] C.-E. Bardyn, M. A. Baranov, C. V. Kraus, E. Rico, A. Imamoglu, P. Zoller, and S. Diehl, “Topology by dissipation,” *New J. Phys.* **15**, 085001 (2013).
- [5] T. Oka and S. Kitamura, “Floquet Engineering of Quantum Materials,” *Annual Review of Condensed Matter Physics* **10**, 387 (2019).
- [6] A. D. Greentree, C. Tahan, J. H. Cole, and L. C. L. Hollenberg, “Quantum phase transitions of light,” *Nature Physics* **2**, 856 (2006).
- [7] M. J. Hartmann, F. G. S. L. Brandão, and M. B. Plenio, “Strongly interacting polaritons in coupled arrays of cavities,” *Nature Physics* **2**, 849 (2006).
- [8] D. E. Chang, V. Gritsev, G. Morigi, V. Vuletić, M. D. Lukin, and E. A. Demler, “Crystallization of strongly interacting photons in a nonlinear optical fibre,” *Nature Physics* **4**, 884 (2008).
- [9] J. Koch, A. A. Houck, K. L. Hur, and S. M. Girvin, “Time-reversal-symmetry breaking in circuit-QED-based photon lattices,” *Phys. Rev. A* **82**, 043811 (2010).
- [10] A. Petrescu, A. A. Houck, and K. Le Hur, “Anomalous Hall effects of light and chiral edge modes on the kagomé lattice,” *Phys. Rev. A* **86**, 053804 (2012).
- [11] J. Cho, D. G. Angelakis, and S. Bose, “Fractional Quantum Hall State in Coupled Cavities,” *Phys. Rev. Lett.* **101**, 246809 (2008).
- [12] R. O. Umucalilar and I. Carusotto, “Artificial gauge field for photons in coupled cavity arrays,” *Phys. Rev. A* **84**, 043804 (2011).
- [13] M. Hafezi, M. D. Lukin, and J. M. Taylor, “Nonequilibrium fractional quantum Hall state of light,” *New J. Phys.* **15**, 063001 (2013).
- [14] M. C. Rechtsman, J. M. Zeuner, Y. Plotnik, Y. Lumer, D. Podolsky, F. Dreisow, S. Nolte, M. Segev, and A. Szameit, “Photonic Floquet topological insulators,” *Nature* **496**, 196 (2013).
- [15] J. Otterbach, M. Moos, D. Muth, and M. Fleischhauer, “Wigner Crystallization of Single Photons in Cold Rydberg Ensembles,” *Phys. Rev. Lett.* **111**, 113001 (2013).
- [16] I. Carusotto and C. Ciuti, “Quantum fluids of light,” *Rev. Mod. Phys.* **85**, 299 (2013).
- [17] K. Le Hur, L. Henriot, A. Petrescu, K. Plekhanov, G. Roux, and M. Schiró, “Many-body quantum electrodynamics networks: Non-equilibrium condensed matter physics with light,” *Comptes Rendus Physique* **17**, 808 (2016).
- [18] C. Noh and D. G. Angelakis, “Quantum simulations and many-body physics with light,” *Rep. Prog. Phys.* **80**, 016401 (2017).
- [19] M. J. Hartmann, “Quantum simulation with interacting photons,” *J. Opt.* **18**, 104005 (2016).
- [20] M. Schiró, C. Joshi, M. Bordyuh, R. Fazio, J. Keeling, and H. Türeci, “Exotic Attractors of the Nonequilibrium Rabi-Hubbard Model,” *Phys. Rev. Lett.* **116**, 143603 (2016).
- [21] M. Fitzpatrick, N. M. Sundaresan, A. C. Y. Li, J. Koch, and A. A. Houck, “Observation of a dissipative phase transition in a one-dimensional circuit qed lattice,” *Phys. Rev. X* **7**, 011016 (2017).
- [22] J. M. Fink, A. Dombi, A. Vukics, A. Wallraff, and P. Domokos, “Observation of the photon-blockade breakdown phase transition,” *Phys. Rev. X* **7**, 011012 (2017).
- [23] A. A. Houck, H. E. Türeci, and J. Koch, “On-chip quantum simulation with superconducting circuits,” *Nature Physics* **8**, 292 (2012).
- [24] S. Schmidt and J. Koch, “Circuit QED lattices: Towards quantum simulation with superconducting circuits,” *Ann. Phys. (Berlin)* **525**, 395 (2013).
- [25] I. Bloch, J. Dalibard, and S. Nascimbène, “Quantum simulations with ultracold quantum gases,” *Nature Physics* **8**, 267 (2012).
- [26] J. G. Bohnet, B. C. Sawyer, J. W. Britton, M. L. Wall, A. M. Rey, M. Foss-Feig, and J. J. Bollinger, “Quantum spin dynamics and entanglement generation with hundreds of trapped ions,” *Science* **352**, 1297 (2016).
- [27] S. Diehl, A. Tomadin, A. Micheli, R. Fazio, and P. Zoller, “Dynamical phase transitions and instabilities in open atomic many-body systems,” *Phys. Rev. Lett.* **105**, 015702 (2010).
- [28] L. M. Sieberer, S. D. Huber, E. Altman, and S. Diehl, “Dynamical Critical Phenomena in Driven-Dissipative Systems,” *Phys. Rev. Lett.* **110**, 195301 (2013).
- [29] T. E. Lee, S. Gopalakrishnan, and M. D. Lukin, “Unconventional magnetism via optical pumping of interacting spin systems,” *Phys. Rev. Lett.* **110**, 257204 (2013).
- [30] J. Jin, D. Rossini, R. Fazio, M. Leib, and M. J. Hartmann, “Photon solid phases in driven arrays of nonlinearly coupled cavities,” *Phys. Rev. Lett.* **110**, 163605 (2013).
- [31] J. Marino and S. Diehl, “Driven Markovian Quantum Criticality,” *Phys. Rev. Lett.* **116**, 070407 (2016).
- [32] O. Scarlatella, R. Fazio, and M. Schiró, “Emergent finite frequency criticality of driven-dissipative correlated lattice bosons,” *Phys. Rev. B* **99**, 064511 (2019).
- [33] C. S. Munoz, B. Buča, J. Tindall, A. González-Tudela, D. Jaksch, and D. Porras, “Spontaneous freezing in driven-dissipative quantum systems,” arXiv preprint arXiv:1903.05080 (2019).
- [34] H.-P. Breuer and F. Petruccione, *The theory of open quantum systems*, 1st ed. (Oxford University Press, USA, 2002).
- [35] T. E. Lee, H. Häffner, and M. C. Cross, “Antiferromagnetic phase transition in a nonequilibrium lattice of Rydberg atoms,” *Phys. Rev. A* **84**, 031402 (2011).
- [36] J. Qian, G. Dong, L. Zhou, and W. Zhang, “Phase diagram of Rydberg atoms in a nonequilibrium optical lattice,” *Phys. Rev. A* **85**, 065401 (2012).
- [37] M. Marcuzzi, E. Levi, S. Diehl, J. P. Garrahan, and I. Lesanovsky, “Universal Nonequilibrium Properties of Dissipative Rydberg Gases,” *Phys. Rev. Lett.* **113**, 210401 (2014).
- [38] C. Carr, R. Ritter, C. G. Wade, C. S. Adams, and K. J. Weatherill, “Nonequilibrium phase transition in a dilute rydberg ensemble,” *Phys. Rev. Lett.* **111**, 113901 (2013).
- [39] F. Letscher, O. Thomas, T. Niederprüm, M. Fleis-

- chhauer, and H. Ott, “Bistability versus metastability in driven dissipative rydberg gases,” *Phys. Rev. X* **7**, 021020 (2017).
- [40] C. D. Parmee and N. R. Cooper, “Phases of driven two-level systems with nonlocal dissipation,” *Phys. Rev. A* **97**, 053616 (2018).
- [41] J. Jin, D. Rossini, R. Fazio, M. Leib, and M. J. Hartmann, “Photon solid phases in driven arrays of nonlinearly coupled cavities,” *Phys. Rev. Lett.* **110**, 163605 (2013).
- [42] J. Jin, D. Rossini, M. Leib, M. J. Hartmann, and R. Fazio, “Steady-state phase diagram of a driven QED-cavity array with cross-Kerr nonlinearities,” *Phys. Rev. A* **90**, 023827 (2014).
- [43] M. Foss-Feig, P. Niroula, J. T. Young, M. Hafezi, A. V. Gorshkov, R. M. Wilson, and M. F. Maghrebi, “Emergent equilibrium in many-body optical bistability,” *Phys. Rev. A* **95**, 043826 (2017).
- [44] M. Biondi, G. Blatter, H. E. Türeci, and S. Schmidt, “Nonequilibrium gas-liquid transition in the driven-dissipative photonic lattice,” *Phys. Rev. A* **96**, 043809 (2017).
- [45] C.-K. Chan, T. E. Lee, and S. Gopalakrishnan, “Limit-cycle phase in driven-dissipative spin systems,” *Phys. Rev. A* **91**, 051601 (2015).
- [46] R. M. Wilson, K. W. Mahmud, A. Hu, A. V. Gorshkov, M. Hafezi, and M. Foss-Feig, “Collective phases of strongly interacting cavity photons,” *Phys. Rev. A* **94**, 033801 (2016).
- [47] H. Spohn, “An algebraic condition for the approach to equilibrium of an open n -level system,” *Letters in Mathematical Physics* **2**, 33 (1977).
- [48] F. Minganti, A. Biella, N. Bartolo, and C. Ciuti, “Spectral theory of liouvillians for dissipative phase transitions,” *Phys. Rev. A* **98**, 042118 (2018).
- [49] H. Weimer, “Variational Principle for Steady States of Dissipative Quantum Many-Body Systems,” *Phys. Rev. Lett.* **114**, 040402 (2015).
- [50] M. Biondi, S. Lienhard, G. Blatter, H. E. Türeci, and S. Schmidt, “Spatial correlations in driven-dissipative photonic lattices,” *New J. Phys.* **19**, 125016 (2017).
- [51] J. Jin, A. Biella, O. Viyuela, L. Mazza, J. Keeling, R. Fazio, and D. Rossini, “Cluster mean-field approach to the steady-state phase diagram of dissipative spin systems,” *Phys. Rev. X* **6**, 031011 (2016).
- [52] A. J. Daley, “Quantum trajectories and open many-body quantum systems,” *Adv. Phys.* **63**, 77 (2014).
- [53] T. Prosen and M. Žnidarič, “Matrix product simulations of non-equilibrium steady states of quantum spin chains,” *J. Stat. Mech.* **2009**, P02035 (2009).
- [54] J. J. Mendoza-Arenas, S. R. Clark, S. Felicetti, G. Romero, E. Solano, D. G. Angelakis, and D. Jaksch, “Beyond mean-field bistability in driven-dissipative lattices: Bunching-antibunching transition and quantum simulation,” *Phys. Rev. A* **93**, 023821 (2016).
- [55] F. Vicentini, F. Minganti, R. Rota, G. Orso, and C. Ciuti, “Critical slowing down in driven-dissipative Bose-Hubbard lattices,” *Phys. Rev. A* **97**, 013853 (2018).
- [56] J. Jin, A. Biella, O. Viyuela, C. Ciuti, R. Fazio, and D. Rossini, “Phase diagram of the dissipative quantum ising model on a square lattice,” *Phys. Rev. B* **98**, 241108 (2018).
- [57] A. Kshetrimayum, H. Weimer, and R. Orús, “A simple tensor network algorithm for two-dimensional steady states,” *Nature Comm.* **8**, 1291 (2017).
- [58] Z. Cai and T. Barthel, “Algebraic versus Exponential Decoherence in Dissipative Many-Particle Systems,” *Phys. Rev. Lett.* **111**, 150403 (2013).
- [59] K. Macieszczak, M. Guță, I. Lesanovsky, and J. P. Garrahan, “Towards a Theory of Metastability in Open Quantum Dynamics,” *Phys. Rev. Lett.* **116**, 240404 (2016).
- [60] “See supplemental material.”
- [61] H. Landa, M. Schiró, and G. Misguich, “In preparation.”
- [62] E. Mascarenhas, H. Flayac, and V. Savona, “Matrix-product-operator approach to the nonequilibrium steady state of driven-dissipative quantum arrays,” *Phys. Rev. A* **92**, 022116 (2015).
- [63] U. Schollwöck, “The density-matrix renormalization group in the age of matrix product states,” *Annals of Physics* **326**, 96 (2011), january 2011 Special Issue.
- [64] M. P. Zaletel, R. S. K. Mong, C. Karrasch, J. E. Moore, and F. Pollmann, “Time-evolving a matrix product state with long-ranged interactions,” *Phys. Rev. B* **91**, 165112 (2015).
- [65] G. Benenti, G. Casati, T. Prosen, D. Rossini, and M. Žnidarič, “Charge and spin transport in strongly correlated one-dimensional quantum systems driven far from equilibrium,” *Phys. Rev. B* **80**, 035110 (2009).
- [66] *ITensor Library*, <http://itensor.org> (version 2.1).
- [67] K. Bidzhiev and G. Misguich, “Out-of-equilibrium dynamics in a quantum impurity model: Numerics for particle transport and entanglement entropy,” *Phys. Rev. B* **96**, 195117 (2017).
- [68] E. Stoudenmire and S. R. White, “Studying Two-Dimensional Systems with the Density Matrix Renormalization Group,” *Annu. Rev. Condens. Matter Phys.* **3**, 111 (2012).
- [69] D. C. Rose, K. Macieszczak, I. Lesanovsky, and J. P. Garrahan, “Metastability in an open quantum Ising model,” *Phys. Rev. E* **94**, 052132 (2016).
- [70] W. Casteels, R. Fazio, and C. Ciuti, “Critical dynamical properties of a first-order dissipative phase transition,” *Phys. Rev. A* **95**, 012128 (2017).
- [71] D. Porras and J. I. Cirac, “Effective quantum spin systems with trapped ions,” *Phys. Rev. Lett.* **92**, 207901 (2004).
- [72] A. Friedenauer, H. Schmitz, J. T. Glueckert, D. Porras, and T. Schaetz, “Simulating a quantum magnet with trapped ions,” *Nature Physics* **4**, 757 (2008).
- [73] C. Schneider, D. Porras, and T. Schaetz, “Experimental quantum simulations of many-body physics with trapped ions,” *Reports on Progress in Physics* **75**, 024401 (2012).
- [74] R. Islam, C. Senko, W. C. Campbell, S. Korenblit, J. Smith, A. Lee, E. E. Edwards, C.-C. J. Wang, J. K. Freericks, and C. Monroe, “Emergence and Frustration of Magnetism with Variable-Range Interactions in a Quantum Simulator,” *Science* **340**, 583 (2013).
- [75] J. Smith, A. Lee, P. Richerme, B. Neyenhuis, P. W. Hess, P. Hauke, M. Heyl, D. A. Huse, and C. Monroe, “Many-body localization in a quantum simulator with programmable random disorder,” *Nature Physics* **12**, 907 (2016).